

Dynamics and Evolution of Toroidal Vortices by Analog Models



Sergey Belyakin^{1*} and Sergey Shuteev^{1,2}

¹Department of General Physics, Physics Faculty, Lomonosov Moscow State University, Moscow, Russia

²Laboratory of dynamic systems, Physics Faculty, Lomonosov Moscow State University, Moscow, Russia

Submission: December 12, 2019; Published: February 05, 2020

*Corresponding author: Sergey Belyakin, Department of General Physics, Physics Faculty, Lomonosov Moscow State University, Moscow, Russia

Abstract

In this paper we consider the possibility of using analog models to study the behavior of the evolution and dynamics of toroidal vortex flows. The current model based on coupled van der Pol generators is used as the main one. In this robot, based on nonlinear dynamics display Bernoulli presented the evolution of the Torah. The use of analog models makes it possible to trace the dynamics of vortex flows.

Keywords: Nonlinear Dynamic System; Toroidal Vortices; Display Bernoulli; Analog Models

Introduction

To obtain toroidal vortex, a vortex flow generator is used (Figure 1). In the first part (Figure 1) a vortex generator with toroidal flow evolution is presented, in the second part of Figure 1 a toroidal vortex in a stable dynamic state is presented. In the third part (Figure 1). the bifurcation of a toroidal vortex is presented. Geometric constructions of hyperbolic attractors the Smale-Williams Attractor [1-3] is presented in Figure 2. The mathematical theory of chaos, based on a strict axiomatic Foundation, deals with strange attractors of the hyperbolic type (Figure 2). In such an attractor, all orbits belonging to it in the phase space of the system are saddle, and stable and unstable

manifolds (invariant sets composed of trajectories approaching the original one in forward or reverse time) intersect transversally, i.e. without touching. Hyperbolic strange attractors are robust (structurally stable). This means the insensitivity of the nature of the movements and the relative position of the trajectories in phase space with respect to the variation of the equations of the system. In contrast to the hyperbolic attractor, quasi-attractors are characterized by a sensitive dependence of dynamics details on parameters. It is clearly desirable for potential applications of chaos such as communication, masking of signals, etc. Thus, from a fundamental and applied point of view it is interesting to realize hyperbolic chaos in physical systems.

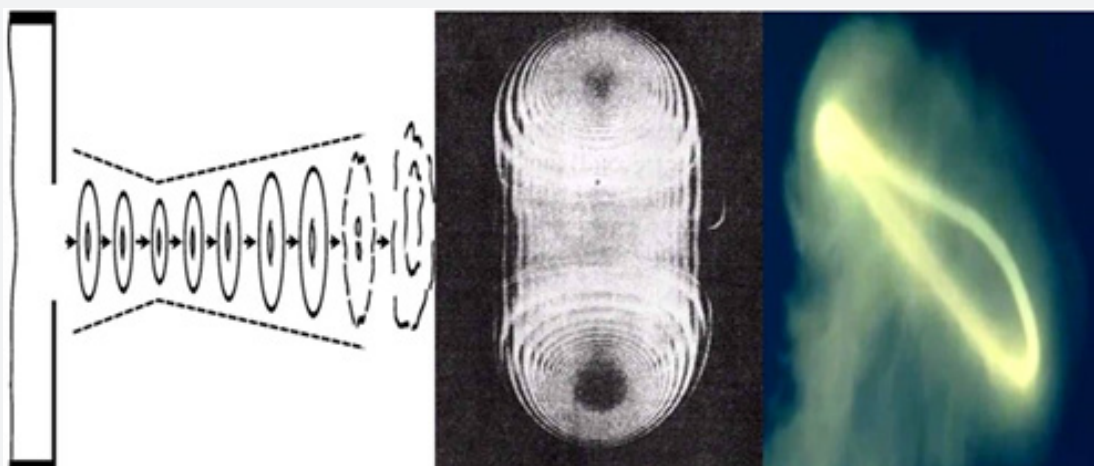


Figure 1: Vortex generator with toroidal flow evolution. A toroidal vortex in a stable dynamic state. Bifurcation of a toroidal vortex.

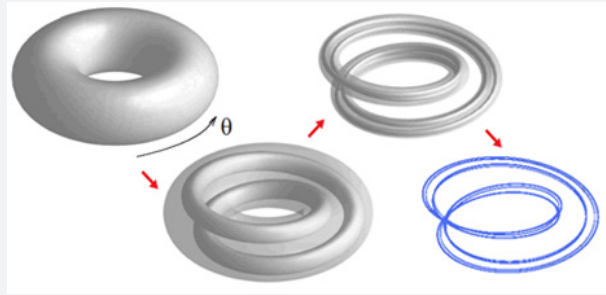


Figure 2: Evolution of a strange attractor of hyperbolic type.

In textbooks and monographs on nonlinear dynamics, examples of hyperbolic attractors are represented by abstract constructions. For example, the Sale-Williams attractor is constructed to map three-dimensional space into itself, defined by the following procedure. Consider a region in the form of a torus, stretch it in length, fold it in half and enclose it in the original torus, as shown in the figure. At each next iteration the number of " turns " doubles. An object that is obtained within the limit of a large number of iterations is called a Smale – Williams solenoid. Its transverse structure has the form of a Cantor set [4 -7].

If we introduce the angular coordinate of the image point q , then on successive iterations it obviously obeys the Bernoulli map $q_{n+1}=\{2q_n\}$. In the remaining two directions, the phase volume element undergoes compression. Therefore, a system of coupled

non-Autonomous generators appears to be a suitable candidate for the implementation of the Smale - Williams attractor. Consider the one-dimensional map: $x_{n+1}=\{2x_n\}$, where the braces denote the fractional part of the number. Its graph and diagram, illustrating the dynamics over several iterations, is shown in Figure 3. It is convenient to represent the variable x in the binary notation, with the digit 0 in the first position after the dividing point corresponds to the location of the representing point in the left, and 1 - in the right half of the unit interval. Suppose, for example, one step of evolution in time is that the sequence of zeros and ones is shifted to the left by one position, and the figure that is on the left side of the dividing point is discarded, and so on. This transformation of the binary sequence, consisting in the shift of all characters by one position, called Bernoulli shift.

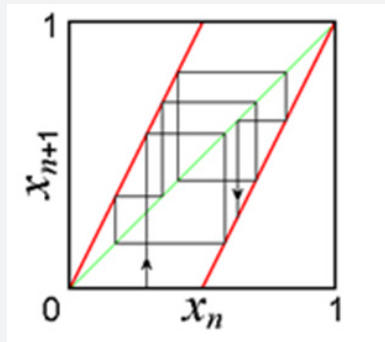


Figure 3: A one-dimensional map $x_{n+1}=\{2x_n\}$, where braces denote the fractional part of the number, the graph and chart illustrate the dynamics over several iterations.

We define the initial state of the random sequence of digits, for example, obtained by flipping coins, according to the rule of the eagle is 0, tails are 1: $x_0 = 0.0101101$. Then, in iterations, the image point will visit the left or right half of the unit interval exactly following our random sequence, thus creating chaos. It is clear that the small perturbation of the initial condition is doubled in one iteration step. Therefore, the Lyapunov exponent for this map is $\ln 2 = 0.693$. How to implement the dynamics corresponding to the Bernoulli map in a physical system. Let us turn to the one shown in Figure 4 flowchart. It is a non-Autonomous oscillatory system based on two oscillators with characteristic frequencies ω_0 and

$2\omega_0$. The parameter controlling the excitation of one and the other oscillator slowly changes in time in antiphase with period T , which is an integer number of periods of the fundamental frequency: $T = 2\pi N/\omega_0$. Thus, alternately excited one, then the other generator. The effect of the first generator on the second is produced through a nonlinear quadratic element. The generated second harmonic serves as a seed when the second generator is excited. In turn, the second generator acts on the first through a nonlinear element that mixes the incoming signal and the auxiliary reference signal at a frequency ω_0 . In this case, a component appears at the difference frequency.

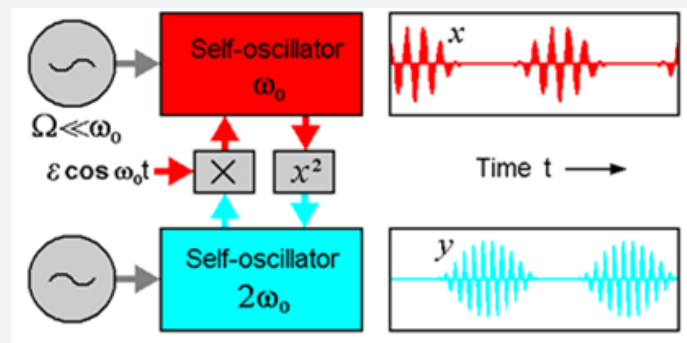


Figure 4: Non-Autonomous oscillatory system based on two oscillators with characteristic frequencies ω_0 and $2\omega_0$.

It resonates with the first generator and serves as a seed when it begins to generate. Both generators, as it were, in turn transmit excitation to one another. Let us explain why the scheme functions as a chaos generator. Suppose that at the generation stage of the first oscillator the oscillations have some phase φ . The signal at the output of the coupling element contains a second harmonic, and its phase 2φ is transmitted to the second oscillator when it begins to generate. By mixing with the reference signal on the second coupling element, the doubled phase is transferred to the original frequency range, so that when the first oscillator is excited, at the

next generation stage, it will receive a phase of 2φ . At successive stages of excitation of the first generator for its phase normalized to 2π , $\theta = \varphi/2\pi$, the Bernoulli map will be valid: $\theta_{n+1} = \{2\theta_n\}$. To observe the described mechanism numerically, we consider a system of equations (1), two van Der Pol oscillators with variable coefficients:

$$\begin{aligned} \ddot{x} - (A \cos 2\pi t / T - x^2)\dot{x} + \omega_0^2 x &= \varepsilon y \cos \omega_0 t \\ \ddot{y} - (-A \cos 2\pi t / T - y^2)\dot{y} + \omega_0^2 y &= \varepsilon x^2 \dots (1) \end{aligned}$$

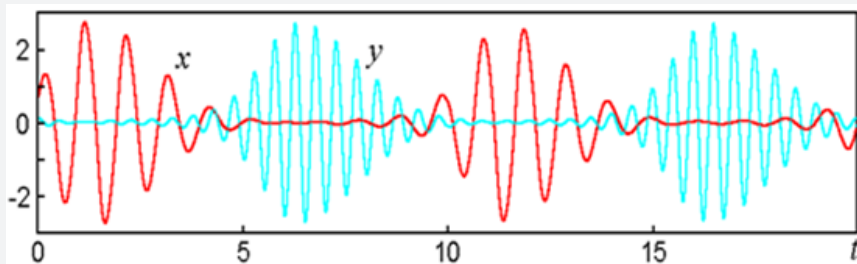


Figure 5: The time dependence of the variables x and y in this system, which performs chaotic motion during relay excitation transfer from one oscillator to another at $\omega_0 = 2\pi$, $T = 10$, $A = 3$, $\varepsilon = 0.5$, is shown.

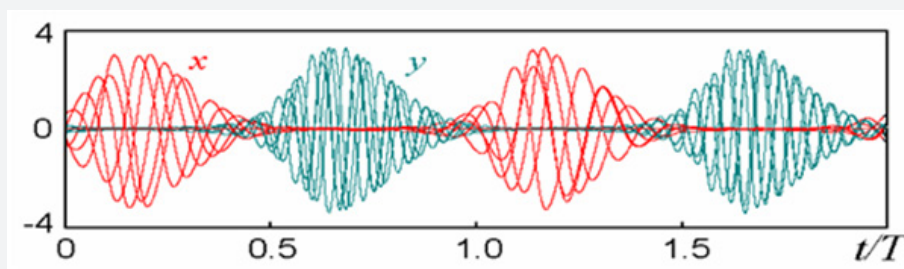


Figure 6: The time dependence of the variables x and y in this system, which performs chaotic motion during relay transfer of excitation from one oscillator to another at $\omega_0 = 2\pi$, $T = 6$, $A = 5$, $\varepsilon = 0.5$, is shown.

For Figure 5 shows the time dependence of the variables x and y in this system, which performs chaotic motion during relay transmission of excitation from one oscillator to another. The graph is based on the results of the numerical solution of the

equations for $\omega_0 = 2\pi$, $T = 10$, $A = 3$, $\varepsilon = 0.5$. For Figure 6 shows the time dependence of the variables x and y in this system, making a chaotic motion in the relay transmission of excitation from one oscillator to another. The graph is based on the results of the

numerical solution of the equations for $\omega_0 = 2\pi$, $T = 6$, $A = 5$, $\varepsilon = 0.5$. Chaos manifests itself in a random walk of the maxima and minima of the filling relative to the envelope. Below is an empirical mapping diagram for the phase of the first oscillator in the middle of the excitation stages. Figure 7 shows the points (θ_n, θ_{n+1}) for a sufficiently large number of t periods. So, we obtain a map which, despite having some deformations, is topologically equivalent to the Bernoulli map $\theta_{n+1} = \{2\theta_n\}$. In fact, if we vary the initial phase so that the image point once bypassed the full circle, the point-image will make a two-fold circumnavigation of the circle. This is expressed in the fact that the graph has two branches located in

the same way as in the first figure at the beginning of this page. The correspondence with the classical Bernoulli map becomes better with increasing the period ratio of N . For Figure 8 a graph of the dependence of the higher Lyapunov exponent (Λ) for a system of coupled non-Autonomous van der Pol oscillators on the amplitude of the slow modulation A at fixed other parameters is presented, and the T period t is taken as a unit of time. As you can see, in a wide range of the parameter, the Lyapunov exponent remains almost constant and is approximately equal to $\ln 2 = 0.693$, which corresponds to the Bernoulli map. At small A the correspondence disappears - the Lyapunov exponent becomes noticeably smaller.

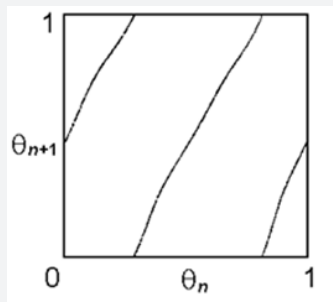


Figure 7: Points (θ_n, θ_{n+1}) are postponed at sufficiently large number of periods T .

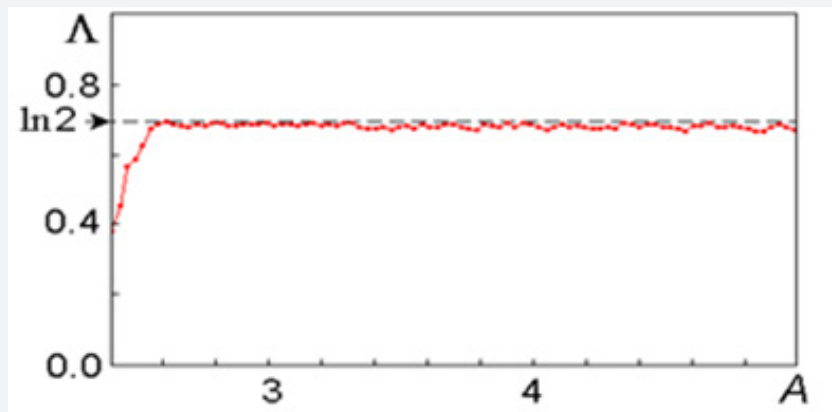


Figure 8: A graph of the dependence of the higher Lyapunov exponent (Λ), for a system of coupled non-Autonomous van der Pol oscillators on the amplitude of the slow modulation A at fixed other parameters is presented.

Summary

There are several approaches to the design of systems with a hyperbolic attractor, such as dynamics at short pulses, the construction of dynamics as a sequence of separate stages, manipulating the excitation phases distributed between alternately excited oscillators, parametric oscillators and oscillators with feedback delay. Finally, some of our proposed systems can be implemented, for example, in electronics, mechanics and nonlinear optics. Opens the possibility of physical realization of hyperbolic chaos, prospects for the application of hyperbolic theory have existed since a purely mathematical discipline.

Current model based on coupled van Der Pol generators

Let us turn to the scheme of the radio engineering device shown in Figure 9 [2,8]. Each of the two subsystems - generators contains an oscillatory circuit formed by an inductor $L_{1,2}$ and a capacitance $C_{1,2}$, and the natural frequency of the second is twice as large as the first. The negative resistance $-R_{1,2}$ is introduced by the element based on the operational amplifier. The increase in energy losses with increasing vibration amplitude is provided by a nonlinear element composed of semiconductor diodes (D). The field-effect transistor introduces a positive conductivity, the value of which is regulated by the voltage supplied to the gate.

It slowly changes in time with a period T in the opposite phase for the first and second generator, which ensures their alternate excitation. The first generator acts on the second through a nonlinear quadratic element A_1 , generating a second harmonic, and the second on the first through a nonlinear element A_2 , mixing the second harmonic and the auxiliary signal at a frequency ω_0

$= 1/\sqrt{L_1 C_1}$ and $2\omega_0 = 1/\sqrt{L_2 C_2}$. We present the dynamics of the proposed scheme for each subsystem and write the Kirchhoff equation (2), expressing the equality of zero total current in the parallel branches of the scheme equation, linking the voltage and current through the inductor:

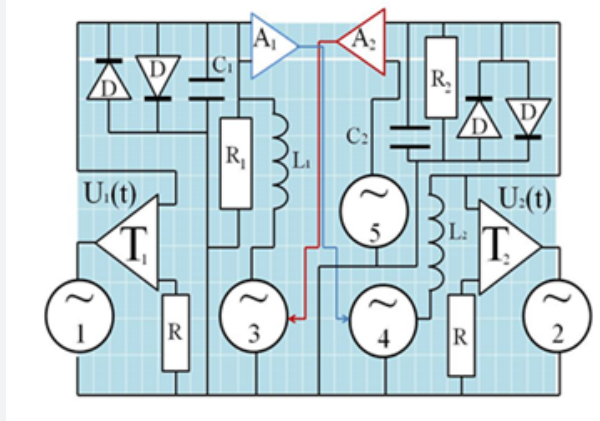


Figure 9: The scheme of the radio engineering device, which is a non-Autonomous oscillatory system assembled on the basis of two subsystems of van Der Pol oscillators with periodically changing parameters.

$$C_1 \frac{dU_1}{dt} = -I_1 + \frac{U_1}{R_1} - f(U_1) - U_1 \left(q_1 - k_1 a \cos \frac{\omega_0 t}{N} \right)$$

$$L_1 \frac{dI_1}{dt} = U_1 + k_2 U_2 \cos \omega_0 t$$

$$C_2 \frac{dU_2}{dt} = -I_2 + \frac{U_2}{R_2} - f(U_2) - U_2 \left(q_2 + k_2 a \cos \frac{\omega_0 t}{N} \right)$$

$$L_2 \frac{dI_2}{dt} = U_2 + k_1 U_1^2 \dots (2)$$

In equation (2), the function $f(U) \approx \alpha U + \beta U^3$ characterizes the current - voltage dependence for a nonlinear element composed of semiconductor diodes (D), $k_{1,2}$ - the transmission coefficients in the circuits providing the connection between the two subsystems. The factor $q \pm ka \cos(\omega_0 t/N)$ corresponds to the conductivity introduced into the circuit by a field-effect transistor in the presence of an alternating gate voltage $\pm a \cos(\omega_0 t/N)$. After replacement of variables providing reduction to the dimensionless form,

$$\tau = \frac{\omega_0 t}{2\pi}, x = U_1 \sqrt{\frac{6\pi\beta}{\omega_0 C_1}}, u = I_1 \sqrt{\frac{6\pi\beta}{\omega_0^3 C_1^3}}$$

$$y = U_2 \sqrt{\frac{6\pi\beta}{\omega_0 C_2}}, v = I_2 \sqrt{\frac{3\pi\beta}{2\omega_0^3 C_2^3}}$$

$$A_1 = \frac{2\pi k_1 a}{\omega_0 C_1}, A_2 = \frac{2\pi k_2 a}{\omega_0 C_2}, \varepsilon_1 = k_1 \sqrt{\frac{\omega_0^3 C_1^3}{6\pi\beta C_2}}, \varepsilon_2 = k_2 \sqrt{\frac{C_2}{C_1}}$$

$$h_1 = \frac{2\pi}{\omega_0 C_1} \left(\frac{1}{R_1} - \alpha - q_1 \right), h_2 = \frac{2\pi}{\omega_0 C_2} \left(\frac{1}{R_2} - \alpha - q_2 \right)$$

receive:

$$\dot{x} = -2\pi u + \left(h_1 + A_1 \cos \frac{2\pi t}{N} \right) x - \frac{1}{3} x^3$$

$$\dot{u} = 2\pi(x + \varepsilon_2 y \cos 2\pi t)$$

$$\dot{y} = -4\pi v + \left(h_2 + A_2 \cos \frac{2\pi t}{N} \right) y - \frac{1}{3} y^3$$

$$\dot{v} = 4\pi(y + \varepsilon_1 x^2) \dots (3)$$

In equation (3) dimensionless variables x and u characterize the voltage and current in the oscillating circuit of the first generator (respectively, U_1 and I_1), and y and v - voltage and current in the second oscillating circuit (U_2 and I_2). Time is normalized for the period of natural oscillations of the primary circuit. Parameters A_1 and A_2 determine the amplitude of the slow modulation of the parameter responsible for the Andronov - Hopf bifurcation in the first and second oscillator, and h_1 and h_2 determine the offset of the mean value of this parameter relative to the bifurcation point. Finally, ε_1 and ε_2 are the communication parameters between subsystems. The system described (Figure 9) was implemented as a laboratory device, with the natural frequencies of the oscillating circuits being approximately 1090 and 2180 Hz. Voltages U_1 and U_2 , respectively, removed from the first and second circuits, could be fed to the recording

equipment (oscilloscope, spectrum analyzer) or entered into the computer in the form of a time series through an analog-to-digital Converter. The time derivative was obtained as a result of analog differentiation using a standard differentiation chain containing a capacitance, resistor, and operational amplifier. Pair in Figure 10 shows portraits of the attractor projected onto a plane where the generalized coordinate (stress) and velocity (time derivative of

stress) for the oscillator are plotted along the coordinate axes at $N = 8$. A color portrait of the attractor was photographed directly from the oscilloscope screen. The second portrait is obtained from solving equations on a computer. It is represented in red tones, where the brightness of the image is proportional to the relative residence time at the corresponding points.

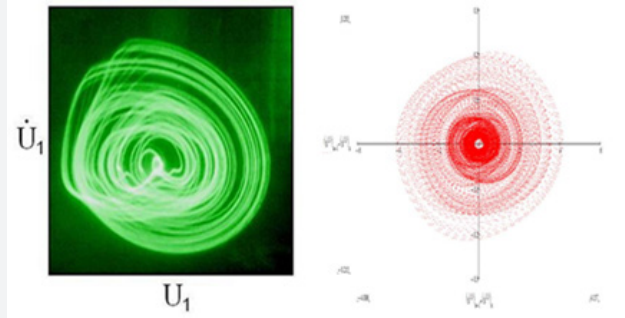


Figure 10: On the left is a photo from the oscilloscope screen of the attractor portrait projected onto the plane of the dynamic variables of the first oscillator (U_1, \dot{U}_1). To the right is the phase portrait of $(x_{n+1} - x_n, x_{n+1} + x_n)$ when the value of the parameters $N = 8, A_1 = 1.5, A_2 = 6, \epsilon_1 = \epsilon_2 = 0.1, h_1 = h_2 = 0$.

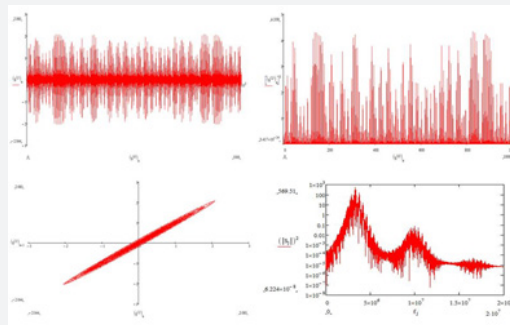


Figure 11: On the left is a photo from the oscilloscope screen of the attractor portrait projected onto the plane of the dynamic variables of the first oscillator (U_1, \dot{U}_1). To the right is the phase portrait of $(x_{n+1} - x_n, x_{n+1} + x_n)$ when the value of the parameters $N = 8, A_1 = 1.5, A_2 = 6, \epsilon_1 = \epsilon_2 = 0.1, h_1 = h_2 = 0$.

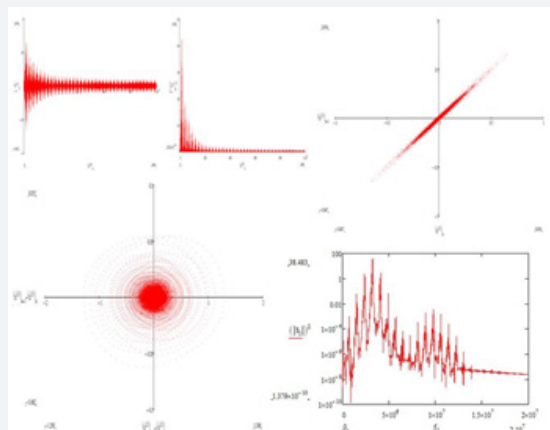


Figure 12: The upper figure shows the time dependences $y(t)$ and $v(t)$ on the left, the phase dependences (y, \dot{y}) and (v, \dot{v}) on the right. The lower figure shows left to right time dependences $x(t), x^2(t)$ and $(x_n - x_{n+1}, x_n + x_{n+1})$, at the bottom $(x_n - x_{n+1}, x_n + x_{n+1})$ and Fourier spectrum. At the value $N = 4, A_1 = 1.5, A_2 = 6, \epsilon_1 = \epsilon_2 = 0.1, h_1 = h_2 = 0$.

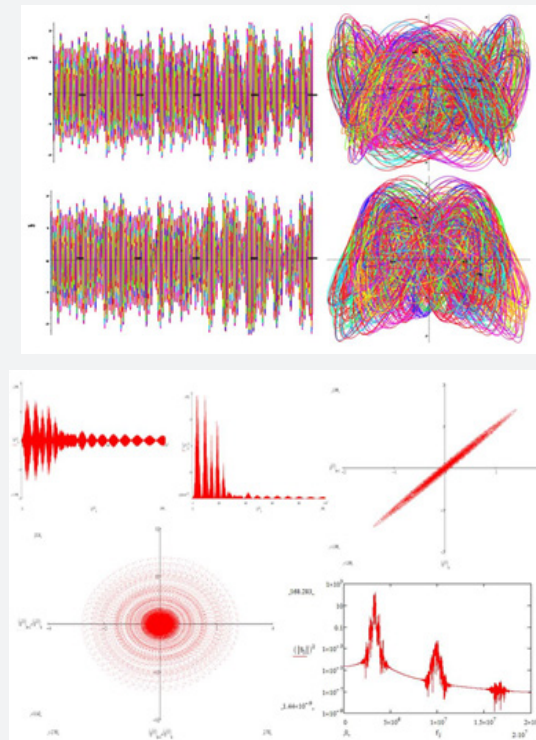


Figure 13: The upper figure shows the time dependencies $y(t)$ and $v(t)$ on the left, the phase dependencies (y, \dot{y}) and (v, \dot{v}) on the right. The lower figure shows left to right time dependencies $x(t)$, $x_2(t)$ and (x_n, x_{n+1}) , at the bottom $(x_n - x_{n+1}, x_n + x_{n+1})$ and Fourier spectrum. At the value $N = 8$, $A_1 = 0.8$, $A_2 = 0.2$, $\epsilon_1 = \epsilon_2 = 0.1$, $h_1 = h_2 = 0$.

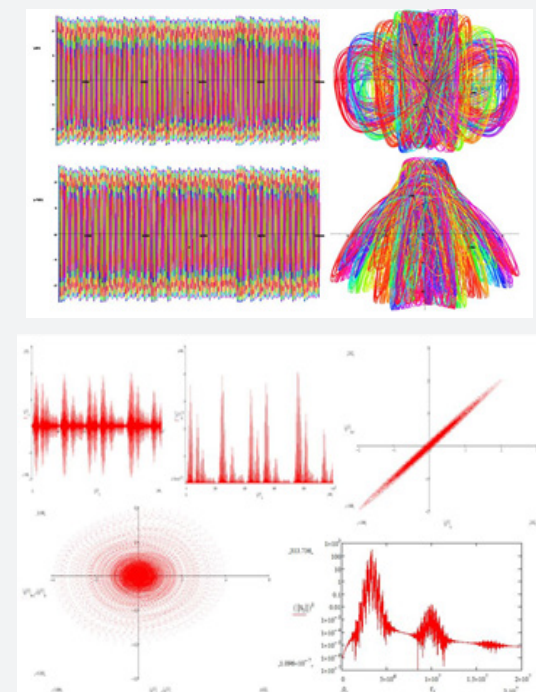


Figure 13: The upper figure shows the time dependencies $y(t)$ and $v(t)$ on the left, the phase dependencies (y, \dot{y}) and (v, \dot{v}) on the right. The lower figure shows left to right time dependencies $x(t)$, $x_2(t)$ and (x_n, x_{n+1}) , at the bottom $(x_n - x_{n+1}, x_n + x_{n+1})$ and Fourier spectrum. At the value $N = 8$, $A_1 = A_2 = 1.5$, $\epsilon_1 = \epsilon_2 = 0.1$, $h_1 = h_2 = 0$.

In the experiment, with proper selection of parameters, chaotic oscillations were observed in the system due to relay transmission of excitation from one oscillator to another. For Figure 11 typical samples of time dependences of voltage in the mode of regular generation of hyperbolic chaos in this subsystem are shown at the ratio of frequency of slow change of parameters at $N = 8$ and Figure 12 frequencies of the auxiliary signal $N = 4$ of multiple bifurcation, - in experiment and by results of the numerical solution of system of the equations. The experimental graph is built on a computer using time series recorded in memory, obtained by analog-to-digital conversion of voltages $U_1(t)$ and $U_2(t)$. For Figure 13 typical samples of time dependences of voltage in the mode of chaotic generation in this subsystem are shown at the ratio of frequency of slow change of parameters at $N = 8$ and Figure 14 signal frequencies $N=8$ with equal amplitudes $A_1 = A_2 = 1.5$, a complex irregular pattern of hyperbolic chaos generation in this subsystem was observed.

Resume

In General, the presented results allow us to confidently assert that both in the experiment and in the theoretical consideration we are dealing with the same object - a strange attractor of the Smale – Williams type in a non-Autonomous oscillatory system. The available data suggest that it is an attractor of hyperbolic type, although, strictly speaking, this statement needs mathematical proof. The appearance of an example of a physical system with a hyperbolic chaotic attractor is of fundamental importance for the further development of nonlinear dynamics and its applications. This is, in a sense, a “breakthrough into the hyperbolic realm.” Based

on the inherent property of coarseness of hyperbolic attractors, we can build other examples of systems with hyperbolic chaos. The presence of such physical systems opens up opportunities for the application of a deeply studied branch of mathematics – hyperbolic theory, and also translates into practice the problem of comparative study of hyperbolic and non-hyperbolic chaos in theory and experiment. This system can be used to study toroidal vortex processes.

References

1. Kuznetsov SP (2005) Example of a Physical System with a Hyperbolic Attractor of the Smale-Williams Type. *Phys Rev Lett* 95: 144101.
2. Kuznetsov SP (2011) Dynamical chaos and uniformly hyperbolic attractors: from mathematics to physics. *UFN* 51(2): 121-149.
3. Kuznetsov SP (2006) Chaotic dynamics in a physical system with a strange Smale – Williams attractor. *JETP* 2: 400-412.
4. Kuznetsov SP (2012) A system of three non-Autonomous oscillators with hyperbolic chaos. A model with dynamics on the attractor described by the mapping on the torus “Arnold’s cat”. *Izvestiya vuzov. Applied nonlinear dynamics* 20(6): 56-66.
5. Grebogi C, Ott E, Pelikan S, Yorke JA (1984) Strange attractors that are not chaotic. *Physica D: Nonlinear Phenomena* 13(1): 261-268.
6. Hunt BR, Ott (2001) Fractal properties of robust strange nonchaotic attractors. *Phys Rev Lett* 87(25): 254101.
7. Kuznetsov SP (2007) On the possibility of realization in the physical system of the strange non-chaotic attractor hunt and Ott. *JTP* 77(4): 10-18.
8. Isaeva OB, Yu A, Jalnina, Kuznetsov SP (2006) Arnold’s cat map dynamics in a system of coupled nonautonomous van der Pol oscillators. *Phys Rev E* 74: 046207.



This work is licensed under Creative Commons Attribution 4.0 License
DOI: [10.19080/ARR.2020.05.555668](https://doi.org/10.19080/ARR.2020.05.555668)

Your next submission with Juniper Publishers will reach you the below assets

- Quality Editorial service
- Swift Peer Review
- Reprints availability
- E-prints Service
- Manuscript Podcast for convenient understanding
- Global attainment for your research
- Manuscript accessibility in different formats
(Pdf, E-pub, Full Text, Audio)
- Unceasing customer service

Track the below URL for one-step submission
<https://juniperpublishers.com/online-submission.php>